Noname manuscript No.
(will be inserted by the editor)

Glassforming liquids, amorphous and semicrystalline polymers: exploring their energy landscape and dynamical heterogeneity by multi-frequency high-field EPR

Vasile Bercu · Carlo Andrea Massa · Silvia Pizzanelli · Luca Pardi · Dino Leporini · Massimo Martinelli

Received: date / Accepted: date

Abstract We review past and recent work carried out on viscous liquids, amorphous and semicrystalline polymers by multifrequency high-field Electron Paramagnetic Resonance (HF-EPR) facility in Pisa. The emphasis is on the enhanced ability to provide fine details of the reorientation process of the paramagnetic guest, the spin probe, revealing features driving the dynamics of the host system, including the energy barrier distribution of glassy polymers and the dynamical heterogeneity of viscous liquids and semicrystalline polymers.

Keywords glassforming liquids · amorphous and semicrystalline polymers · energy landscape · dynamical heterogeneity · high-field Electron Paramagnetic Resonance

PACS 64.70.Pf · 76.30.-v · 61.25.Hq

V. Bercu
Faculty of Physics, University of Bucharest, Str. Atomistilor 405, Magurele, Jud. Ilfov, Bucharest RO-077125, Romania

C. A. Massa · L. Pardi · D. Leporini
Istituto per i Processi Chimico-Fisici-Consiglio Nazionale delle Ricerche (IPCF-CNR), via G. Moruzzi 1, 56124 Pisa, Italy

S. Pizzanelli
Istituto di Chimica dei Composti OrganoMetallici-Consiglio Nazionale delle Ricerche (ICCOM-CNR), via G. Moruzzi 1, 56124 Pisa, Italy

D. Leporini
Dipartimento di Fisica "Enrico Fermi", Università di Pisa, Largo B. Pontecorvo 3, 56127 Pisa, Italy
E-mail: dino.leporini@unipi.it

M. Martinelli
Livorno, Italy

1 Introduction

The present paper reviews in a concise way the experimental efforts carried out in Pisa by using the high-field Electron Paramagnetic (HF-EPR) spectroscopy to provide novel insight into a wide class of disordered systems both in the solid state, *i.e.* amorphous polymers [1–7], and in the liquid state, *i.e.* glassforming viscous liquids [8,9], polymer melts [8] and semicrystalline polymers [10,11]. For completeness, in addition to the previous studies, we also mention other investigations employing the same equipment [12–18]. The latter studies are not reviewed here.

After a period of technological development started in 1999, the HF-EPR spectrometer setup in Pisa eventually reached the final form reported elsewhere [19], superseding previous versions [20]. Ref. [19] describes the status of the HF-EPR spectrometer in 2002 with its structure, performances and limits (see also [21,22]). In the first decade of the century attempts to implement a Quasi Optical setup were pursued, that finally were abandoned due to the lack of appropriately consistent funding.

Two main issues were addressed, namely the distribution of energy barriers which must be overcome by the spin probe during the reorientation process [1–7] and the spatial distribution of microscopic mobility [10,11]. The former aspect is strictly related to the features of the so called "energy landscape" of glasses, whereas the latter, dubbed "dynamical heterogeneity" [23,24] is a distinctive feature of viscous liquids approaching the solidification process, known as glass transition, and is also present in semicrystalline polymers due to coexistence of liquid and solid fractions.

The next Section presents the background concisely.

2 Background

HF-EPR provides insight into disordered systems due to: i) the remarkable orientation resolution of the spin probes dynamics [25], to be ascribed to the larger magnitude of the anisotropic Zeeman interaction which in turn leads to a wider distribution of resonance frequencies [26,27], ii) the use of spin probes, being well coupled to the guest phase, *e.g.* see [28].

2.1 Glasses and liquids

The solidification of a viscous liquid in a disordered glass is a process - usually referred to as "glass transition" (GT) - where crystallization is largely or totally inhibited by suitable cooling, compression or even chemical reaction [29–31]. On approaching GT from, *e.g.*, higher temperatures, one observes in a limited range a spectacular decrease of the microscopic diffusivity of several orders of magnitude. The mobility loss is signalled by the corresponding huge increase of the viscosity. Interestingly, the familiar Stokes-Einstein (SE) relationship

between diffusivity and the viscosity breaks down close to GT [32,33]. The SE failure is considered as one of the most prominent signatures of the so-called dynamical heterogeneity (DH), *i.e.* the spatial distribution of regions with different mobility [23,24,34].

The development of a microscopic theory of GT based on first principles and no phenomenological assumption is still a subject of intense studies carried out on both atomic and molecular systems, including polymers [35]. A current tool providing a topographic view of viscous liquids and glass formation is the multidimensional landscape of the collective potential energy hypersurface created when a large number of particles interact with one another. This potential energy landscape (PEL) is formed by individual "basins", each containing a local potential energy minimum or "inherent structure", corresponding to some particle arrangement. Transitions between inherent structures involve a series of activated jumps over energy barriers with distribution $g(E)$ [36]. Depending on the temperature, different part of PEL are sensed. At high temperature, the system explore the upper limit of the energy landscape and using the arguments provided by the Central Limit theorem one can expect to find a gaussian shape for $g(E)$. By cooling to the lowest temperatures, the system will begin to explore the deepest lower energy states which are expected to be exponentially distributed following the general arguments of extreme-value statistics [37].

If the particle rearrangements are thermally activated, there is an average (trapping) time $\tau = \tau_0 \exp(E/kT)$ before overcoming the barrier of height E at temperature T, k and τ_0 being the Boltzmann constant and a microscopic time scale, respectively. Therefore, the energy barrier distribution $g(E)$ leads to a trapping time distribution $\rho(\tau)$ [1,2]. If $g(E)$ is gaussian, the distribution $\rho(\tau)$ takes the form of a log-gauss distribution (LGD). If the distribution of barrier heights is exponential with width $\overline{E}$, namely

$$g(E) = \begin{cases} 0 & \text{if } E < E_{min} \\ \frac{1}{\overline{E}} exp(-\frac{E-E_{min}}{\overline{E}}) & \text{if } E \geq E_{min} \end{cases} \tag{1}$$

one finds that $\rho(\tau)$ is expressed by the power-law distribution (PD)

$$\rho_{PD}(\tau) = \begin{cases} 0 & \text{if } \tau < \tau_{PD} \\ x\tau_{PD}^{x}\tau^{-(x+1)} & \text{if } \tau \geq \tau_{PD} \end{cases} \tag{2}$$

with $x = kT/\overline{E}$ and $\tau_{PD} = \tau_0\, exp(E_{min}/kT)$. Note that the absence of energy barriers below E_{min} does not change the shape of $\rho_{PD}(\tau)$ and allows for the temperature dependence of τ_{PD}. If the width of the energy-barriers distribution is vanishingly small, a single reorientation time (SRT) is found with:

$$\rho_{SRT}(\tau) = \delta(\tau - \tau_{SRT}) \tag{3}$$

2.2 Semicrystalline polymers

HF-EPR spectroscopy was used to investigate the reorientation of a spin probe in semicrystalline poly-(dimethylsiloxane) (PDMS) from the glassy region up to the melt. In semicrystalline polymers the macromolecules pack together in ordered regions, the crystallites, which are separated by disordered noncrystalline regions. An intermediate interfacial region, usually referred to as rigid-amorphous fraction (RAF), is also present [38–40]. This region is a disordered constrained environment, whereas the rest of the noncrystalline region other than RAF is expected to exhibit properties like the completely amorphous bulk polymers and is usually termed as mobile amorphous fraction (MAF). Differently from MAF, RAF does not become liquid-like above the glass transition temperature T_g. The confinement of spin probes in the disordered fraction offers the possibility of selective studies of such regions in semicrystalline PDMS with EPR. This is one major advantage of this method considering that the assignment of a relaxation process to the amorphous, crystalline, or interfacial regions of a semicrystalline polymer is a delicate matter[41–48].

Since there is a mobility gradient from MAF to the more constrained RAF, the spin probes are expected to experience a heterogeneous dynamics, with apparent similarities with the case of viscous liquids, tracking MAF and RAF environments. HF-EPR is more well-suited than the usual X-band EPR to discriminate between different distributions of reorientation times.

We used HF-EPR to investigate another issue concerning semicrystalline polymers, *i.e.* reversible crystallization and melting. As a matter of fact, linear and flexible macromolecules exhibit local equilibria between the surfaces of the individual polymer crystallites and the surrounding amorphous regions which are established by thermodynamically reversible structure changes, usually referred to as reversible crystallization and melting [39,40,49]. This phenomenon has been ascribed to the attachment and detachment of segments of partially melted macromolecules which are held at or in the vicinity of the crystal growth face [39,50]. In the case of PDMS, we searched signatures of an equilibrium melting/freezing local process involving RAF and MAF. However, no distinctive spectral features associated with RAF were observed in slowly cooled PDMS. Thus, we adopted an improved strategy to increase the amount of RAF by quench cooling the polymer and were able to detect an exchange process between a fraction of trapped spin probes and a more mobile one.

3 Glasses and liquids

3.1 Glasses: exponential distribution of rotational energy barriers in glassy polystyrene

The focus of our interest was polystyrene (PS) having energy barrier distribution $g(E)$ intensively investigated by different experimental techniques *e.g.,* mechanical relaxation [51], Raman [52], light and neutron scattering [53]. Our

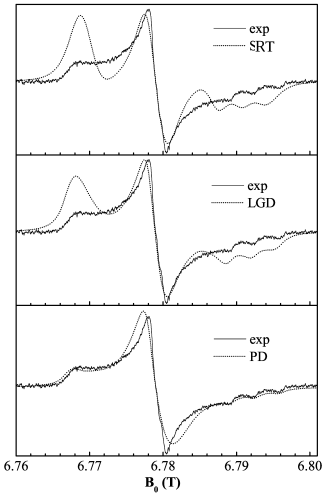

Fig. 1 Best fit of the HF-EPR line shape at 190 GHz of TEMPO spin probe in PS at 270 K by using SRT (Eq.3), LGD and PD (Eq.2). It is assumed that the spin probe undergoes reorientation by a jump angle $\phi = 20°$. Best-fit parameters for PD model: $\tau_{PD} = 0.225$ ns, $x = 0.575$. See ref. [2] for further details.

experiments detected the HF-EPR signal of the spin probe TEMPO [27] and and the results were reported in a first letter [1] and a subsequent extended paper [2]. Notice that TEMPO and the phenyl group of PS have similar shape. TEMPO is stiff with almost spherical shape [54]. It has an average van der Waals radius $r_{TEMPO} = 3.3 \pm 0.2$ Å and may be sketched as an oblate ellipsoid with semiaxes $r_{||} \approx 2.7$ Å and $r_{\perp} \approx 3.7$ Å . Similar small spin probes are anticipated to undergo jump dynamics in glasses [55–57].

Fig. 1 demonstrates that the HF-EPR line shape discriminates between different reorientation models. The PD model is more accurate. The consistency of the analysis is confirmed by Fig.2 showing how close is the distribution of barrier heights sensed, according to the PD model, by TEMPO in glassy PS with the distributions revealed by other techniques.

3.2 Liquids: exploring the energy landscape above T_g

At temperature well above T_g, the most advanced microscopic description of the slowing down observed on approaching GT from above is the mode coupling theory (MCT) which emphasizes the role of the cage in which the molecules are caught for a finite time due to packing constraints [58]. In particular, the ideal MCT (IMCT) predicts the existence of a sharp dynamic crossover, *i.e.*, a transition from liquid-like to solid-like dynamics, at a critical temperature, T_c leading to characteristic scaling laws for density correlations and, particularly, a cusp-like anomaly in the temperature dependence of the non-ergodicity parameter f_q. In terms of energy landscape, It has been sug-

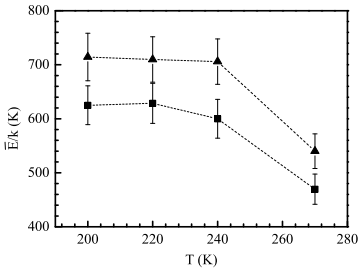

Fig. 2 Temperature dependence of the width $\overline{E}$ of the exponential energy-barrier distribution of TEMPO in glassy PS, eq.1, as detected by HF-EPR at 190 GHz (squares) and 285 GHz (triangles). Previous measurements by internal friction [51], Raman [52] and light scattering [53] yield $\overline{E}_{IF}/k = 760 \pm 40$ K, $\overline{E}_{Raman}/k = 530 \pm 60$ K and $\overline{E}_{LS}/k = 530 \pm 40$ K, respectively. Dotted lines are guides for the eye. See ref. [2] for further details.

gested that T_c demarcates temperatures where the system explores deeper regions of the potential-energy surface from those at which it has access to all regions [59]. Signatures of distinct dynamical regimes in the energy landscape of a glass-forming liquid have been reported [60].

Resorting to the high angular resolution of HF-EPR spectroscopy, a model independent determination of the rotational analogue f_{rot} of the non-ergodicity parameter by using suitable spin probes which couple to the glassy dynamics of the host was carried out [9]. The approach is based on the fact that relatively large spin probes in viscous liquids exhibit HF-EPR line shapes very close to the so called "powder" pattern, being a distinctive feature of nearly immobile paramagnetic molecules [26,27]. However, a closer inspection shows that even in this regime, with spin probe reorientation times roughly between $1 - 10$ ns, the line shape is highly sensitive to the specifics of the reorientation process and its rate [2]. In this respect, an elementary tool to appreciate the HF-EPR sensitivity is the distance ΔB between selected peaks of the line shape corresponding to specific extrema (or saddle points) of the resonating magnetic field of the three hyperfine components of the spectrum (turning points) [2,7].

Our system of interest was the archetypical glassformer o-Terphenyl (OTP) where two sizeable spin probes, ANDRO and NONA where dissolved. The study considered the temperature dependence of the spectral spacing ΔB_{ν_L} recorded at EPR Larmor frequency $\nu_L = 95, 190$ and 285 GHz. Figure 3 shows the results. Four regimes are observed: regime I - at low temperatures ΔB_{ν_L} shows only a minor change; regime II - approaching 280 K a much stronger decrease with temperature sets in which for all frequencies stops at 297.5 ± 0.5 K; regime III - above that temperature a plateau-like feature in ΔB_{ν_L} vs T is observed; regime IV - at the highest temperatures, again a strong decrease is observed, reflecting the onset of the collapse of the line shape due to the faster motion of the spin probe. The collapse is expected to occur at higher temperatures if higher Larmor frequency ν_L is employed. Consequently, the width of the plateau is largest at highest frequency, and this is what is observed. In Fig. 3 the results for the probe molecule NONA are also included,

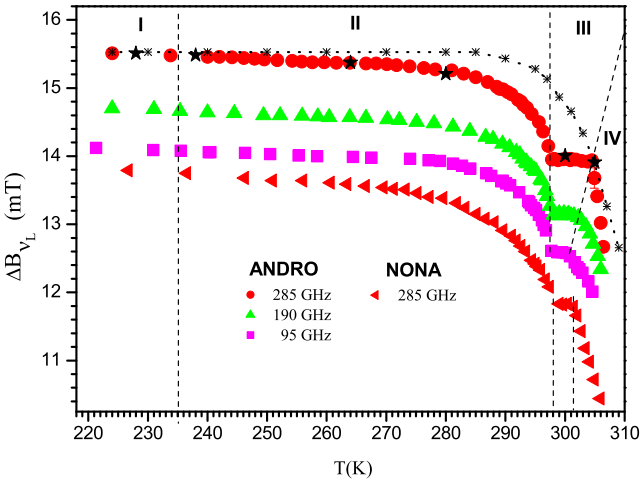

Fig. 3 Temperature dependence of ΔB_{ν_L} of the spin probe ANDRO ($\nu_L = 95, 190, 285$ GHz) and NONA ($\nu_L = 285$ GHz) in OTP. Stars denote points concerning ΔB_{250} from ref. [61]. All curves (but the one denoted by red dots) are shifted vertically to make the comparison easier. Black curves are theoretical simulations [62] of ΔB_{285} approximating ANDRO to a prolate ellipsoid diffusing due to the α-process with either stick (continuous) or slip (dashed) boundary conditions. Notably, neutron scattering experiments reveal the knee at ~ 290 K [63], to be compared with ~ 298 K revealed by HF-EPR. See ref. [9] for further details.

showing the same qualitative behavior. Within experimental accuracy, the same crossover temperature 297.5 ± 0.5 K is observed as by using ANDRO spin probe, providing evidence that the phenomenon is not driven by specific features of the spin probe. The crossover temperature is rather close to the one revealed by neutron scattering at ~ 290 K [63]. We attribute the ΔB_{ν_L} data for regimes I, II and III to a pre-averaging effect due to some motion significantly faster than the structural relaxation. We interpret the decrease of ΔB_{ν_L} as the decrease of pre-averaging effect due to the decreasing amplitude f_{rot} of the fast dynamics which stops above $297.5K$ and thus marks the crossover temperature T_c.

4 Semicrystalline polymers: heterogeneous dynamics

4.1 EPR line shapes

The dynamics of the amorphous fraction in semicrystalline PDMS from the glassy region (below 147 K) up to the melt (above about 230 K) was investigated by HF-EPR [10,11]. Two different thermal protocols, slow and quench cooling, were applied to PDMS obtaining samples, PDMSsc [10] and PDMSq [11], with different amounts of RAF. In fact, quench cooling in the glass region and subsequent reheating to reach the temperature of interest T

($T_g < T < T_m$) leads to larger polycrystallinity than slow cooling from above T_m = melting point down to T [64–66]. The enhancement is understood in terms of both augmented primary nucleation [50] and increased disorder of the crystallite surfaces. The presence of a large number of small irregular crystallites results in a larger surface area of the crystal phase in comparison to the case of large crystallites with regular surfaces obtained upon slow cooling from the melt. The larger interface between melt and crystallites is anticipated to yield a larger amount of RAF, since the RAF thickness is weakly dependent on both the temperature and the crystallinity [38] and nanometric in size [67]. The dynamics of the amorphous fraction of the polymer was investigated monitoring the reorientation of the spin probes TEMPO and methoxy-TEMPO (m-TEMPO) in PDMSsc and PDMSq, respectively. Figure 4 shows selected HF-EPR spectra of the spin probes in PDMS at different temperatures using the irradiating frequencies of 285 and 190 GHz.

The spectra markedly change with the temperature above T_g = 147 K. Upon heating above T_g, the difference between the resonating magnetic field of the most distant peaks ΔB decreases and the line width of the peaks increases (see Figure 4), until the features reminding those of the powder sample are lost around $T_m - 20$ K for PDMSsc. Above that temperature, the motional narrowing of the EPR line shape becomes strong, and a triplet structure starts appearing which sharpens as the temperature is increased. A similar behavior is exhibited by PDMSq, with the exception that the powder features are lost at around $T_m = 230$ K.

4.2 Dynamical heterogeneity of the tracer reorientation

To gain quantitative information on the spin probe reorientation, we adopted the jump model [55,68,69]. In PDMSsc, the spectra below T_g were successfully simulated using the SRT model, Eq.3, whereas above T_g a power-law distribution of reorientation times, Eq.2, is necessary [10]. The failure of the SRT model is anticipated in that it misses any detail on the heterogeneous dynamics occurring in the disordered region between the crystallites. Differently, in PDMSq, the SRT model satisfactorily predicts the line shape up to 200 K and becomes inadequate in the range $200 - 230$ K, where the analysis gives clear indications that the distribution of the rotational mobility of the spin probes has a bimodal structure with (i) a broad component corresponding to spin probes with fast and intermediate mobility, as detected in PDMSsc, and (ii) a narrow component corresponding to spin probes with extremely low mobility, characterized by the reorientation time $\tau_{trapped}$ [11]. The two fractions of the spin probes are expected to be located in the disordered fraction far from the crystallites and trapped close to the crystallites, respectively. In the melt, or even from $T_m - 17$ K for PDMSsc, as discussed below, the high PDMS fluidity averages the distribution of reorientation times quite effectively and narrows considerably the distribution so that the description provided by the SRT model is good enough.

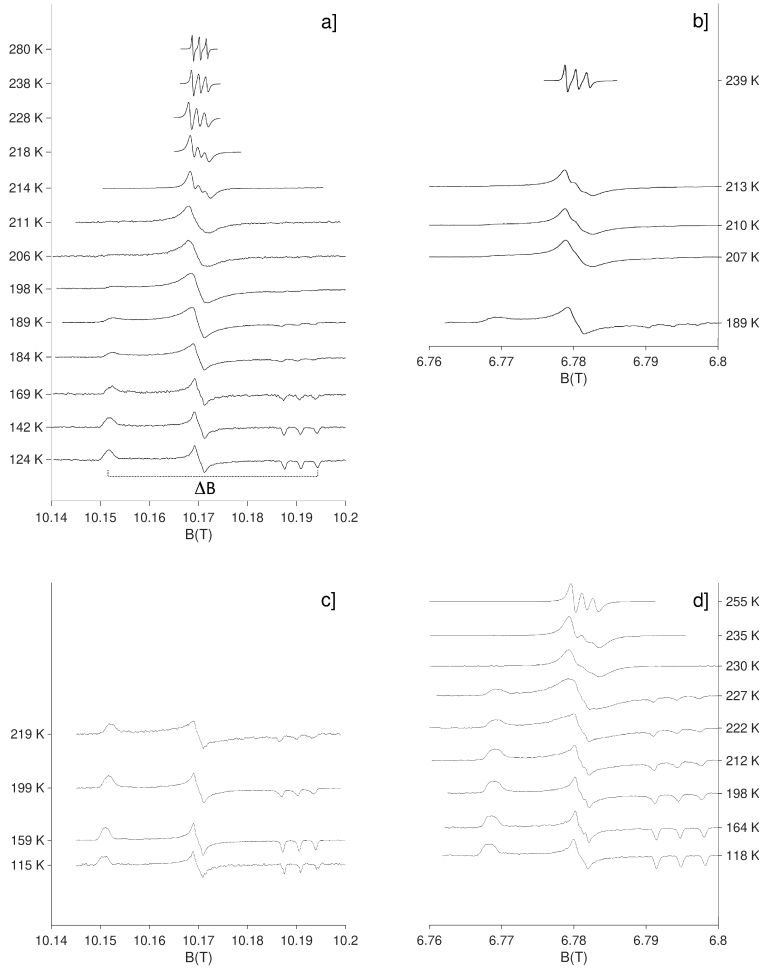

Fig. 4 Selected HF-EPR spectra of TEMPO in PDMSsc (top) [10] and of m-TEMPO in PDMSq (bottom) [11] at different temperatures using the irradiating frequencies of 285 (a,c) and 190 (b,d) GHz. See [10, 11] for further details.

4.3 Evidence of MAF and RAF

Figure 5 shows the temperature dependence of the average reorientation time $\langle\tau\rangle$ as drawn by the HF-EPR data sets recorded at 190 and 285 GHz by using the reorientation time distribution described above. The values of $\langle\tau\rangle$ depend little on the frequency, signaling that the whole distribution of reorientation times is collected by both frequencies. The average reorientation time $\langle\tau\rangle$ decreases slowly as the temperature is increased. For low temperatures, the probe reorientation is accounted for by an Arrhenius law with an activation

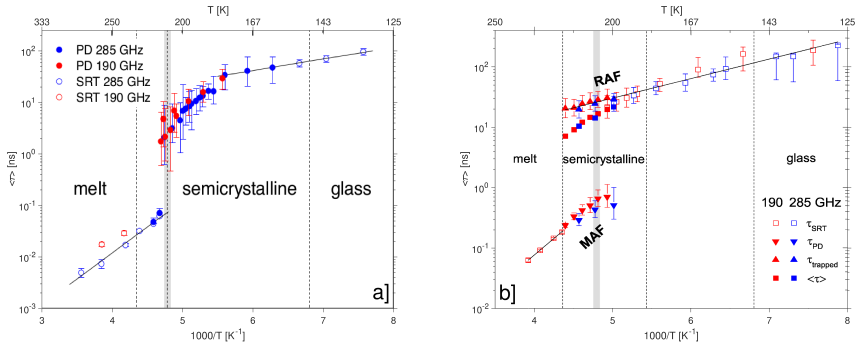

Fig. 5 Temperature dependence of the average reorientation time $\langle\tau\rangle$ of the spin probe in PDMSsc (left-hand side) [10] and in PDMSq (right-hand side) [11]. The dashed vertical lines mark the glass (147 K) and the melting transitions ($\simeq$230 K). The gray region highlights the range of the onset of the PDMS melting ($\simeq$209 K) as detected by DSC. The low temperature and the high-temperature straight lines are Arrhenius fits with activation energies 4.4 $\pm$ 0.3 and 18.8 $\pm$ 0.9 kJ/mol for PDMSsc and 6.2 $\pm$ 0.3 and 20.9 $\pm$ 0.4 kJ/mol for PDMSq.

energy of 4-6 kJ/mol in the two PDMS samples (see Figure 5). Close activation energy values were reported for PDMS investigated by neutron scattering and attributed to CH_3 jumps about the C_3 axis [70,71]. This suggests a good coupling between the probe and local motions rather than the structural relaxation around T_g. The absence of any signature affecting $\langle\tau\rangle$ at T_g suggests that around T_g RAF is larger than MAF. No signature of cold crystallization is also found, thus indicating that the HF-EPR signal of the spin probe does not detect the formation of the crystals occurring on heating during data collection. In PDMSq, the trapped fraction of the spin probes is present between the cold crystallization and T_m, as indicated by the Arrhenius temperature dependence of the reorientation time of the trapped fraction $\tau_{trapped}$, observed up to T_m, which is in ideal continuation of the one of the single reorientation time τ_{SRT} characteristic of the spin probe reorientation at lower temperatures (see Figure 5 b). This is striking evidence that the probe molecules reorienting with the correlation time $\tau_{trapped}$ are located in RAF.

The average reorientation time $\langle\tau\rangle$ drops dramatically at about 213 K, *i.e.* 17 K below T_m, for PDMSsc and at T_m for PDMSq. At these temperatures, the distribution of reorientation times disappears, signaling the softening of RAF, and the SRT model applies. The precocious softening of RAF in PDMSsc might be ascribed to the melting of the thinnest lamellae releasing part of the constraints.

In the melt the temperature dependence of $\langle\tau\rangle$ of the spin probe is described by an Arrhenius law with activation energy about 19 kJ/mol in both samples. The activation energy is comparable to the one of the PDMS segmental dynamics (14.6 kJ/mol [70]); *i.e.*, the spin probe is more coupled to the structural relaxation above the melting temperature than around T_g.

One should notice that the shortest reorientation time of the power distribution, τ_{PD}, approaches smoothly the single reorientation time found at

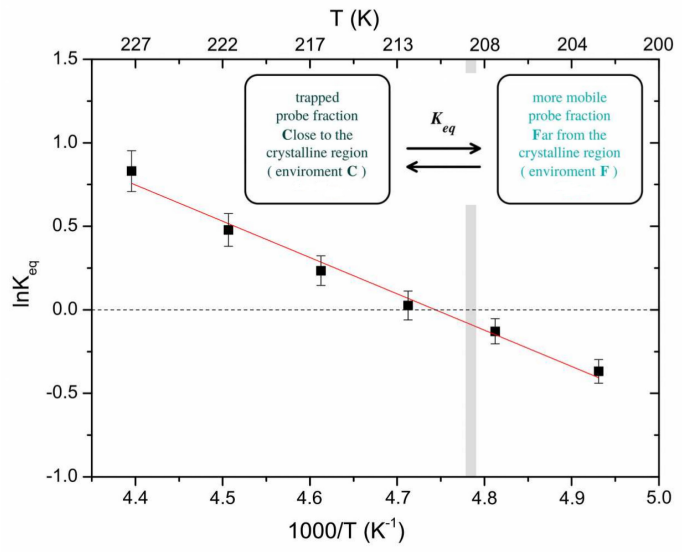

Fig. 6 Van't Hoff plot of the equilibrium constant K_{eq} between the trapped and the more mobile fractions of the spin probe in semicrystalline PDMS, see ref. [11] for details. The straight red line is the best-fit with the equation $K_{eq} = e^{-(\Delta G_r^0/RT)}$ and $\Delta G_r^0 = \Delta H_r^0 - T\Delta S_r^0$. Detrapping involves positive standard enthalpy ($\Delta H_r^0 = 18 \pm 1$ kJ/mol) and entropy ($\Delta S_r^0 = 86 \pm 5$ J/K mol) of reaction. The gray region highlights the range of the onset of PDMS melting according to DSC ($\simeq 209$ K). Notice that detrapping is favored, *i.e.* $\ln K_{eq}$ is positive and ΔG_r^0 is negative, if $T \gtrsim 209$ K. Inset: equilibrium between the fractions of the spin probes trapped and more mobile, being close to and far from the crystalline region, respectively.

temperatures above that where $\langle\tau\rangle$ drops. This is shown for PDMSq in Figure 5 b. This is evidence that the fastest fraction of the spin probes couples to the PDMS segmental motion, revealing the presence of MAF. This fast fraction accelerates without sensing the melting of the polymer.

4.4 Local reversible melting

The larger amount of RAF in PDMSq revealed signatures of reversible local melting [11]. The trapped and the more mobile fractions of the spin probe in the noncrystalline region of the polymer above T_g, described in the paragraph 4.2, are subject to a dynamic exchange process. We tentatively model it as a chemical reaction thermodynamically equilibrated and consider the trapped and the more mobile fractions of the spin probe as the reactant and product, respectively. This scenario is sketched in the inset of Figure 6. The related reaction equilibrium constant is K_{eq}.

Figure 6 presents the van't Hoff plot of the equilibrium constant K_{eq}. It is seen that the detrapping of the spin probe is favored; *i.e.*, K_{eq} is larger than 1, if $T \gtrsim 209$ K, namely at temperatures higher than the onset of PDMS melting as

detected by DSC which occurs at $\simeq 209$ K. Reminding that $K_{eq} = e^{(-\Delta G_r^0/RT)}$, one finds that the best-fit values of the standard Gibbs enthalpy and entropy of reaction drawn from Figure 6 are $\Delta H_r^0 = 18 \pm 1$ kJ and $\Delta S_r^0 = 86 \pm 5$ J/K per mole of spin probe. Assuming that the spin probes are very diluted, it should be observed that these parameters are dominated by the environments of the probe close and far from the crystalline region and much less affected by the coupling of the spin probe with them. Therefore, picturing the environments as crystalline-like and liquid-like, we explore the proportionality betweeen the van't Hoff parameters ΔH_r^0 and ΔS_r^0 with the enthalpy and entropy of fusion per repeating PDMS unit, ΔH_m and ΔS_m, respectively.

$$\Delta H_r^0 = z_H \, \Delta H_m \tag{4}$$

$$\Delta S_r^0 = z_S \, \Delta S_m \tag{5}$$

where z_H and z_S are suitable constants depending on the microscopic features of the exchange process. We take $\Delta H_m = 4.619$ kJ/mol and $\Delta S_m = 19.6$ J/K mol as listed in [72]. These values are in good agreement with a recent NMR study ($\Delta H_m = 4.54$ kJ/mol [73]) and alternative sources ($\Delta S_m = 19.1$ J/(K mol) [74]). One finds $z_H = 3.9$ and $z_S = 4.4$ from eq 5; *i.e.*, the structural change of the surroundings of the spin probe from the trapped to the more mobile state is equivalent to the one of reversible melting of about z $\simeq$ 4 PDMS monomers.

References

1. V. Bercu, M. Martinelli, C.A. Massa, L. Pardi, D. Leporini, J. Phys.: Condens. Matter **16**, L479 (2004)
2. V. Bercu, M. Martinelli, C.A. Massa, L.A. Pardi, D. Leporini, J. Chem. Phys. **123**, 174906 (2005)
3. V. Bercu, M. Martinelli, C.A. Massa, L.A. Pardi, D. Leporini, Europhys. Lett. **72**, 590 (2005)
4. V. Bercu, M. Martinelli, C.A. Massa, L.A. Pardi, D. Leporini, J. Non-Cryst. Solids **352**, 5029 (2006)
5. V. Bercu, M. Martinelli, C.A. Massa, L.A. Pardi, D. Leporini, Philos. Mag. **87**, 795 (2007)
6. V. Bercu, M. Martinelli, C.A. Massa, L.A. Pardi, D. Leporini, Appl. Magn. Reson. **33**, 365 (2008)
7. V. Bercu, M. Martinelli, C.A. Massa, L.A. Pardi, D. Leporini, Z. Phys. Chem. **226**, 1379 (2012)
8. V. Bercu, M. Martinelli, C.A. Massa, L.A. Pardi, D. Leporini, J. Optoelectron. Adv. M. **9**, 1785 (2007)
9. V. Bercu, M. Martinelli, C.A. Massa, L.A. Pardi, E. Rössler, D. Leporini, J. Chem. Phys. **129**, 081102 (2008)
10. C.A. Massa, S. Pizzanelli, V. Bercu, L. Pardi, D. Leporini, Macromolecules **47**, 6748 (2014)
11. C.A. Massa, S. Pizzanelli, V. Bercu, L. Pardi, D. Leporini, Macromolecules **50**, 5061 (2017)
12. M. Martinelli, C.A. Massa, L. Pardi, V. Bercu, F.F. Popescu, Phys. Rev. B **67**, 014425 (2004)

13. A. Caneschi, A. Dei, D. Gatteschi, C.A. Massa, L.A. Pardi, S. Poussereau, L. Sorace, Chem. Phys. Lett. **371**, 694 (2003)
14. F.F. Popescu, M. Martinelli, C.A. Massa, L.A. Pardi, V. Bercu, Magn. Reson. Chem. **43**, S215 (2005)
15. F.F. Popescu, V. Bercu, J.N. Barascu, M. Martinelli, C.A. Massa, L.A. Pardi, M. Stefan, S.V. Nistor, M. Nikl, P. Bohacek, J. Chem. Phys. **128**, 034505 (2008)
16. F.F. Popescu, V. Bercu, J.N. Barascu, M. Martinelli, C.A. Massa, L.A. Pardi, M. Stefan, S.V. Nistor, M. Nikl, Opt. Mater. **32**, 570 (2010)
17. F. DiBenedetto, D. Borrini, A. Caneschi, G. Fornaciai, M. Innocenti, A. Lavacchi, C.A. Massa, G. Montegrossi, O. W, L.A. Pardi, M. Romanelli, Phys. Chem. Miner. **38**, 483 (2011)
18. F. DiBenedetto, A. Buccianti, G. Montegrossi, M. Innocenti, C.A. Massa, L.A. Pardi, M. Romanelli, Amer. Miner. **97**, 1619 (2012)
19. L.C. Brunel, A. Caneschi, A. Dei, D. Friselli, D. Gatteschi, A.K. Hassan, L. Lenci, M. Martinelli, C.A. Massa, L.A. Pardi, F. F.Popescu, I. Ricci, L. Sorace, Res. Chem. Intermed. **28**, 215 (2002)
20. G. Annino, M. Cassettari, M. Fittipaldi, L. Lenci, I. Longo, M. Martinelli, C.A. Massa, L.A. Pardi, Appl. Magn. Reson. **506**, 495 (2000)
21. D. Friselli, C.A. Massa, M. Martinelli, L. Pardi, I. Ricci, Inorg. Chim. Acta **361**, 4164 (2008)
22. L. Lenci, M. Martinelli, C.A. Massa, L.A. Pardi, I. Ricci, A.K. Hassan, A. Caneschi, L.C. Brunel, Appl. Magn. Reson. **21**, 607 (2001)
23. M.D. Ediger, Annu. Rev. Phys. Chem. **51**, 99 (2000)
24. R. Richert, J. Phys.: Condens. Matter **14**, R703 (2002)
25. D. Leporini, V. Schädler, U. Wiesner, H.W. Spiess, G. Jeschke, J. Chem. Phys. **119**, 11829 (2003)
26. L.J. Berliner, Spin labeling: Theory and Applications, Academic, New York (1976)
27. L.J. Berliner, J. Reuben, Biological magnetic resonance, Plenum, New York **8** (1989)
28. M. Faetti, M. Giordano, D. Leporini, L. Pardi, Macromolecules **32**, 1876 (1999)
29. C. Angell, J.Non-Crystalline Sol. **131-133**, 13 (1991)
30. P.G. Debenedetti, Metastable Liquids: Concepts and Principles. Princeton University Press, Princeton N.J. pp. xiv, 411 (1996)
31. K.L. Ngai, *Relaxation and Diffusion in Complex Systems* (Springer, Berlin, 2011)
32. I. Chang, F. Fujara, B. Geil, G. Heuberger, T. Mangel, H. Sillescu, Journal of Non-Crystalline Solids **172-175**, 248 (1994)
33. J. Douglas, D. Leporini, J. Non-Cryst. Solids **235-237**, 137 (1998)
34. H. Sillescu, Journal of Non-Crystalline Solids **243**(2), 81 (1999)
35. L. Berthier, G. Biroli, Rev. Mod. Phys. **83**, 587 (2011)
36. F.H. Stillinger, *Energy Landscapes, Inherent Structures, and Condensed-Matter Phenomena* (Princeton University Press, Princeton USA, 2015)
37. C. Monthus, J.P. Bouchaud, J. Phys. A: Math. Gen. **29**, 3847 (1996)
38. G.R. Strobl, The Physics of Polymers, 3rd ed.; Springer: Berlin (2007)
39. B. Wunderlich, Prog. Polym. Sci. **28**, 383 (2003)
40. G. Strobl, Prog. Polym. Sci. **31**, 398 (2006)
41. K.U. Kirst, F. Kremer, V.M. Litvinov, Macromolecules **26**, 975 (1993)
42. K. Schmidt-Rohr, H.W. Spiess, Multidimensional Solid-State NMR and Polymers; Academic Press: London (1994)
43. R.F. Boyer, Polymer **17**, 996 (1976)
44. P. Törmälä, J. Macromol. Sci., Polym. Rev. **17**, 297 (1979)
45. N.G. McCrum, B.E. Read, G. Williams, Anelastic and Dielectric Effects in Polymeric Solids; Dover Publications: New York (1991)
46. K.L. Ngai, Relaxation and Diffusion in Complex Systems; Springer: Berlin (2011)
47. K.L. Ngai, C.M. Roland, Macromolecules **26**, 2688 (1993)
48. L. Larini, A. Barbieri, D. Prevosto, P.A. Rolla, D. Leporini, J. Phys.: Condens. Matter **17**, L199 (2005)
49. A. Wurm, M. Merzlyakov, C. Schick, J. Therm. Anal. Calorim. **60**, 807 (2000)
50. B. Wunderlich, Thermal Analysis of Polymeric Materials; Springer: Berlin (2005)
51. K.A. Topp, D.G. Cahill, Z. Phys. B **101**, 235 (1996)

52. A.P. Sokolov, V.N. Novikov, B. Strube, Europhys. Lett. **38**, 49 (1997)
53. N.V. Surovtsev, J.A.H. Wiedersich, V.N. Novikov, E. Rössler, A.P. Sokolov, Phys. Rev. B **58**, 14888 (1998)
54. A. Barbieri, G. Gorini, D. Leporini, Phys. Rev. E **69**, 061509 (2004)
55. L. Andreozzi, F. Cianflone, C. Donati, D. Leporini, J. Phys.: Condens. Matter **8**, 3795 (1996)
56. J. Kim, T. Keyes, J. Chem. Phys. **121**, 4237 (2004)
57. C. De Michele, D. Leporini, Phys. Rev. E **63**, 036702 (2001)
58. W. Götze, *Complex Dynamics of Glass-Forming Liquids: A Mode-Coupling Theory* (Oxford University Press, Oxford, 2008)
59. C.A. Angell, Complex Behavior in Glassy Systems, Eds M. Rubi, C. Perez-Vicente, Springer, Berlin pp. 1–21 (1997)
60. S. Sastry, P.G. Debenedetti, F.H. Stillinger, Nature **393**, 554 (1998)
61. K.A. Earle, J.K. Moscicki, A. Polimeno, J.H. Freed, J. Chem. Phys. **106**, 9996 (1997)
62. M. Giordano, P. Grigolini, D. Leporini, P. Marin, Phys. Rev. A **28**, 2474 (1983)
63. A. Tölle, H. Schober, J. Wuttke, F. Fujara, Phys. Rev. E **56**, 809 (1997)
64. H. Meyer, In Polymer Crystallization: Obervations Concepts and Interpretations; Reiter, G., Sommer, J.-U., Eds.; Springer: Berlin **10** (2008)
65. X. Wang, J. Ouyang, Int. J. Chem. Eng. Appl. **6**, 2831 (2015)
66. H. St-Onge, IEEE Trans. Electr. Insul. **EI-15**, 359 (1980)
67. L. Mandelkern, The Crystalline State. In Physical Properties of Polymers, 3rd ed.; Cambridge University Press: Cambridge, UK pp. 209–315 (2004)
68. E. Ivanov, N. Sov. Phys. JETP **18**, 1041 (1964)
69. L. Alessi, L. Andreozzi, M. Faetti, D. Leporini, J. Chem. Phys. **114**, 36313639 (2001)
70. V. Arrighi, S. Gagliardi, C. Zhang, F. Ganazzoli, J.S. Higgins, R. Ocone, M.T.F. Telling, Macromolecules **36**, 8738 (2003)
71. H.H. Grapengeter, B. Alefeld, R. Kosfeld, Colloid Polym. Sci. **265**, 226 (1987)
72. L. Mandelkern, R.G. Alamo, In Physical Properties of Polymers Handbook, II Ed.; Mark, J. E., Ed.; Springer, Berlin pp. 165–186 (2007)
73. A. Maus, K. Saalwächter, Macromol. Chem. Phys. **208**, 2066 (2007)
74. V.P. Privalko, J. Phys. Chem. **84**, 3307 (1980)